Printed in U.S.A.

77-JPGC-NE-21

an ASME publication

$3.00 PER COPY
$1.50 TO ASME MEMBERS

Analysis of Closely Spaced Double Tubesheets Under Mechanical and Thermal Loadings

Alan I. Soler
Executive Vice President
Holtec International

The field equations governing structural behavior of double tubesheet configurations are formulated using beam-column and plate theory including shear deformation. The resulting system of equations is valid for arbitrary spacing between the tubesheets and includes all component interactions. The twelve coupled first-order ordinary differential equations, involving six force and moment resultants, and six deformation variables, are solved using direct integration. Numerical results are obtained which emphasize the importance of some typical system parameters. Particular attention is focused on shear and bending in the tubes due to differential in-plane thermal growth of the tubesheets.

Contributed by the Nuclear Engineering Division of The American Society of Mechanical Engineers for presentation at the ASME-IEEE Joint Power Generation Conference, Long Beach, Calif., September 18-21, 1977. Manuscript received at ASME Headquarters June 20, 1977.

Copies will be available until June 1, 1978.

THE AMERICAN SOCIETY OF MECHANICAL ENGINEERS, UNITED ENGINEERING CENTER, 345 EAST 47th STREET, NEW YORK, N.Y. 10017

Analysis of Closely Spaced Double Tubesheets Under Mechanical and Thermal Loadings

A. I. SOLER

NOMENCLATURE

L = separation between double tubesheets
d = tube O.D.
E_T = Young's modulus of tube
V_i, N_i, M_i = tubesheet force and moment resultants (Fig. 2)
τ, m, q = tubesheet surface tractions (Fig. 2)
h_i = tubesheet thickness
E_i, ν_i = tubesheet Young's modulus, Poisson's ratio
U_{oi}, w_i, θ_i = tubesheet deformation parameters
F_T, H_T, M_T = tube force and moment resultants
A_T, I_T = geometric parameters of tube
$\{Z\}$ = dependent variable matrix
$[A]$, $\{B\}$, $\{C\}$ = matrices involved in field equation formulation
a = tubesheet radius
r = dependent variable
p_i = applied pressures
T_i = applied tubesheet temperature changes
α_i = tubesheet coefficients of thermal expansion
L_2 = half length of condenser
$\eta_i = E_L^*/E_i$ = ratio of effective Young's modulus (which accounts for tubesheet perforations) to actual Young's modulus

INTRODUCTION

Preventing fluid leakage between shell side and tube side of shell and tube heat exchangers due to tube joint leakage is of prime importance in design of units where intermingling of the component fluids may cause undesirable results. One method to inhibit mixing of component fluids is to provide double tubesheet construction. Double tubesheets have been employed previously in submarine systems. Similar tubesheet construction has often been used where mixing of shell and tube side streams may lead to an explosive mixture.

Prevention of leakage of circulating water into condenser steam space, though always a concern in power plant condenser design, has received renewed attention with the industry trend to all-volatile treatment (AVT) of condensate. It is noted (1)[1] that with an AVT system, even moderate leaks eventually require that all or part of the condensing system be shut down to isolate and repair leakage points. Since outage costs may run in excess of $100,000 to $200,000 per day, elimination of condenser leakage is immediately translated into improved plant economy. Among other items, Reference (1) suggests development of double tubesheet configurations with rolled tubes in lieu of single tubesheets with all welded in place tubes. The use of double tubesheet construction may have an advantage over welding tubes in place because of the problem of maintaining quality control in a large unit having a great number of tube ends to be welded. As discussed in Reference (1), the double tubesheet configuration consists basically of two closely spaced tubesheets, connected by tubes. The configuration may be employed in either U-tube exchangers, floating head exchangers, or in fixed tube exchangers. In the application to large power plant condensers, it is suggested that the gap between the tubesheets be filled with condensate quality water at a pressure greater than that of the circulating water system. Under this condition, any tube

[1] Underlined numbers in parentheses designate References at end of paper.

joint leakage flows from the gap into either the steam or circulating water space so that shell side leakage is noncontaminating.

As shown in Fig. 1, if the spacing, L,

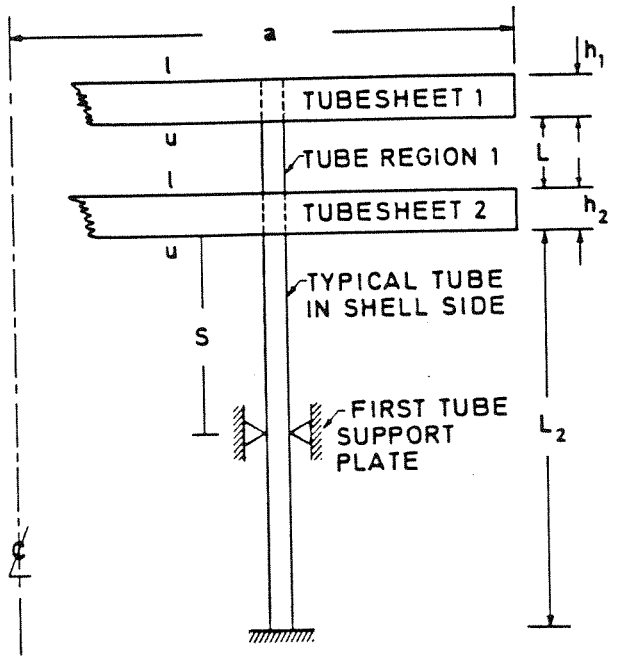

Fig. 1 Double tubesheet configuration

between tubesheets is large, then interaction between tubesheets is minimal, and design of the individual tubesheets to carry the necessary loading is generally carried out without consideration of the adjacent tubesheet. In smaller units, the amount of tubing is not so great that the gap, L, cannot be set large enough so as to minimize interaction between the tubesheets. Generally, a simple but conservative estimate of the minimum distance, L, is obtained from an equation described in Reference (2).

$$L = \left[\frac{3E_m d\Delta}{\sigma_a}\right]^{1/2} \qquad (1)$$

where:

E_m = tube tensile modulus of elasticity
d = tube diameter
σ_a = allowable stress
$\Delta = |\alpha_1 T_1 - \alpha_2 T_2| \ell$.

In the foregoing, Δ represents unrestrained differential in-plane thermal movement between tubesheets that induces lateral tube flexure, α_i are thermal expansion coefficients of the tubesheet materials, and T_i are respective temperature changes from the assembly temperature. The length, ℓ, is the characteristic length over which unrestrained expansion occurs. Equation (1) assumes that the tube is built in at each tubesheet, that the tube accomodates lateral movement at its ends by bending only, and that the effect of tubesheet interaction and tubesheet properties can be ignored. Spacings of 9 to 12 in. generally result from application of equation (1).

The application of the foregoing design equation to set the gap spacing has drawbacks when applied to large units. Alignment problems are evident in assembly, and unit cost may be increased, especially with expensive, corrosive-resisting tube materials, because of the excess tubing which does not contribute to heat transfer capacity. It has been suggested in Reference (1) and by others, that the foregoing problems of double tubesheet design in large units can be eliminated by reducing the gap, L, between tubesheets to the order of 1 in. or less. Such a reduction, however, should not be considered unless appropriate design procedures, which include the interaction between tubesheets, the effect of tube and tubesheet shear as well as bending, and the simultaneous consideration of mechanical and thermal loadings, are developed. Such procedures must be verified and formulated for routine application.

Formulations of the field equations for double tubesheets, which include interaction between adjacent tubesheets, are presented in References (3) and (4). The equations presented in References (3, 4) become inaccurate for gap spacings less than approximately 10 times the tube diameter because shear deformation is not included in thr formulation. Since our interest in this work is directed toward analysis of closely spaced tubesheets having gap spacing on the order of one or two tube diameters, the effect of shear deformation must be included in the field equations. In the following sections, we outline the development of the governing equations and the solution technique employed in the numerical computations. Subsequently, we focus attention on a typical double tubesheet configuration as a vehicle for investigating implications of the tubesheet structural coupling. In the derivation, and in subsequent analysis, we assume axisymmetric loading and geometry. This assumption is in keeping with accepted tubesheet design practice where

the local effects of the perforation array are simply replaced by effective stress and displacement efficiency factors.

THEORETICAL ANALYSIS

Fig. 2 shows an element of tubesheet

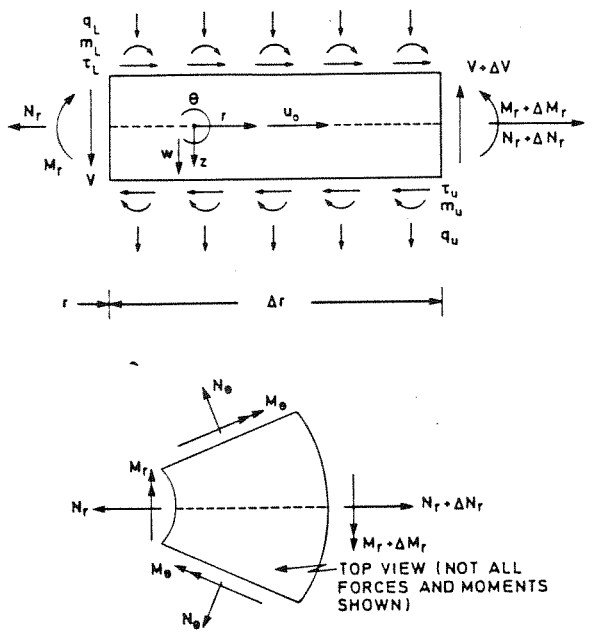

Fig. 2 Tubesheet free body diagram

with the force and moment resultants of classical plate theory, together with surface loadings τ, q, and m defined on the upper and lower surfaces. The equilibrium equations for the tubesheets labeled "one" and "two" in Fig. 1 are obtained as (i=1,2)

$$\frac{dV_i}{dr} + \frac{V_i}{r} = q_{ui} + q_{\ell i} \tag{2}$$

$$\frac{dN_{ri}}{dr} + \frac{N_{ri}-N_{\theta i}}{r} + \tau_{\ell i} - \tau_{ui} = 0 \tag{3}$$

$$\frac{dM_{ri}}{dr} + \frac{M_{ri}-M_{\theta i}}{r} + V_i - (m_{ui}+m_{\ell i} + \frac{h_i}{2}[\tau_{ui} + \tau_{\ell i}]) = 0 \tag{4}$$

For i = 1, 2 we employ the usual deformation assumptions of plate theory

$$u_{ri}(r,z) = U_{oi}(r) + z\theta_i(r); \quad w_z(r,z) = w_i(r) \tag{5}$$

and, after suitable integration of the constitutive equations of linear thermoelasticity, evolve the set of equations

$$N_{ri} + N_i^* = K_i\left(\frac{dU_{oi}}{dr} + \nu_i \frac{U_{oi}}{r}\right) \tag{6}$$

$$N_{\theta i} + N_i^* = K_i\left(\frac{U_{oi}}{r} + \nu_i \frac{dU_{oi}}{dr}\right) \tag{7}$$

i = 1,2

$$M_{ri} + M_i^* = D_i\left(\frac{d\theta_i}{dr} + \nu_i \frac{\theta_i}{r}\right) \tag{8}$$

$$M_{\theta i} + M_i^* = D_i\left(\frac{\theta_i}{r} + \nu_i \frac{d\theta_i}{dr}\right) \tag{9}$$

In equations (6) through (9), we have defined the quantities

$$N_i^* = \frac{E_i\alpha_i}{1-\nu_i}\int_{-\frac{h_i}{2}}^{\frac{h_i}{2}} T_i(r,z)dz; \quad M_i^* = \frac{E_i\alpha_i}{1-\nu_i}\int_{-\frac{h_i}{2}}^{\frac{h_i}{2}} zT_i(r,z)dz$$

$$K_i = \frac{E_i h_i}{1-\nu_i}; \quad D_i = K_i\frac{h_i^2}{12} \tag{10}$$

Equations (6) through (9) can be solved for $N_{\theta i}$, $M_{\theta i}$ directly and yield

$$N_{\theta i} = E_i h_i \frac{U_{oi}}{r} + \nu_i N_{ri} - N_i^*(1-\nu_i) \tag{11}$$

$$M_{\theta i} = \frac{E_i h_i^2}{12}\frac{\theta_i}{r} + \nu_i M_{ri} - M_i^*(1-\nu_i) \tag{12}$$

We assume that the shear resultant, V_i, is related to the plate deformation variables by the simplified equation

$$\frac{dw_i}{dr} = -\theta_i - \frac{6}{5}\frac{V_i}{G_i h_i} \tag{13}$$

G_i is the shear modulus of the i^{th} plate. The neglect of shear deformation to derive a plate theory is equivalent to setting $G_i = \infty$ in equation (13). Note that in each plate, the Young's modulus and Poisson's ratio are reduced to reflect the weakening effect of the perforation array.

We turn now to the determination of the surface loadings, τ, q, m. These loadings involve the applied pressures in the three regions of interest, and also provide the mechanisms for coupling the two tubesheets through the effect of the tubing. Fig. 3 shows a typical deformed tube with force and moment resultants, and kinematic variables defined on the figure. In Reference (5), a stiffness matrix is presented for a beam which includes

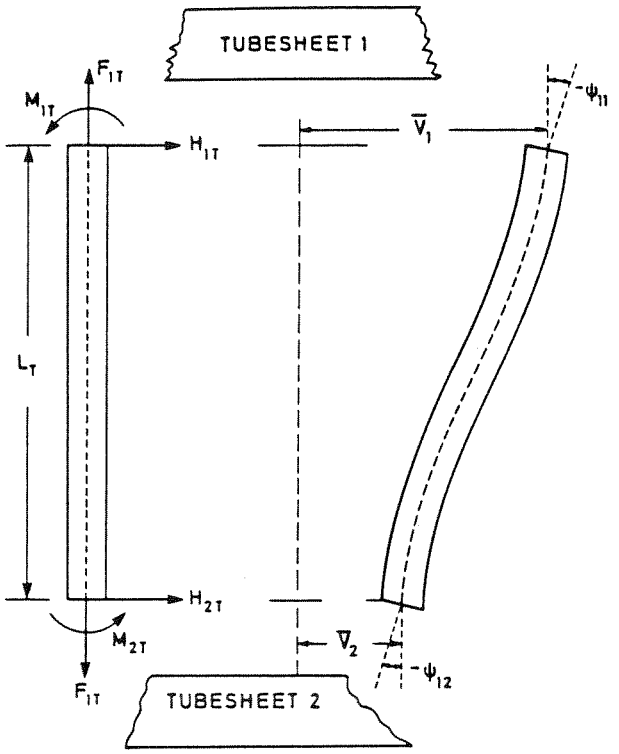

Fig. 3 Tube free body diagram

shear deformation. The relationship between tube shear forces and moments, and tube end displacements and rotations is written in the matrix form.

$$\begin{Bmatrix} H_{1T} \\ M_{1T} \\ H_{2T} \\ M_{2T} \end{Bmatrix} = \gamma \begin{bmatrix} 6 & 3L_T & -6 & +3L_T \\ 3L_T & 2L_T^2(1+3g/L_T^2) & -3L_T & L_T^2(1-6g/L_T^2) \\ -6 & -3L_T & 6 & -3L_T \\ 3L_T & L_T^2(1-6g/L_T^2) & -3L_T & 2L_T^2(1+3g/L_T^2) \end{bmatrix} \begin{Bmatrix} \bar{V}_1 \\ \psi_{11} \\ \bar{V}_2 \\ \psi_{12} \end{Bmatrix} \quad (14)$$

where

$$\gamma = \frac{2E_T I_T/L_T^3}{(1+12g/L_T^2)}; \quad g = 2E_T I_T/G_T A_T \quad (15)$$

and $L_m = L$ for the tubes in region 1 (Fig. 1). E_T, G_m, I_T, A_m are the tube tensile modulus, shear modulus, metal moment of inertia, and metal area, respectively. To represent the effect of tubing between the two tubesheets in Fig. 1, we need only relate forces and moments H_{iT}, M_{iT} to appropriate τ, m, q, in Fig. 2, and relate kinematic variables $\bar{V}$, ψ to appropriate plate deformation quantities.

The effect of the tubing on the shell side of the assemblage is also modeled by equation (14), except that tube shear deformation is neglected. For the shell side region of tubing, we effect the following notation change:

$$\begin{Bmatrix} H_{1T} \\ M_{1T} \\ H_{2T} \\ M_{2T} \end{Bmatrix} \rightarrow \begin{Bmatrix} H_{3T} \\ M_{3T} \\ H_{4T} \\ M_{4T} \end{Bmatrix}; \quad \begin{Bmatrix} \bar{V}_1 \\ \psi_{11} \\ \bar{V}_2 \\ \psi_{12} \end{Bmatrix} \rightarrow \begin{Bmatrix} \bar{V}_3 \\ \psi_{21} \\ \bar{V}_4 \\ \psi_{22} \end{Bmatrix} \quad (16)$$

In the representation of shell side tubing bending and shear, we set L_T in equation (14), equal to S, the span to the first support plate or baffle. If we assume that the presence of the first support plate implies that $\bar{V}_4 = 0$, then it can be shown that

$$H_{3T} = \frac{2E_T I_T}{S^3}(6\bar{V}_3 + 3S[\psi_{21} + \psi_{22}])$$
$$M_{3T} = \frac{2E_T I_T}{S^3}(3S\bar{V}_3 + S^2[2\psi_{21} + \psi_{22}]) \quad (17)$$

To eliminate ψ_{22} from equation (17), we assume that

$$\psi_{22} = \bar{a}\bar{V}_3 + \bar{b}\psi_{21} \quad (18)$$

where $\bar{a}$, $\bar{b}$ are chosen to reflect the presence of the remaining baffles not modeled in Fig. 1. It is shown in Reference (6), that for the case $\bar{V}_3 = 0$, the correct solution may be written as

$$M_{3T} = \frac{F_n E_T I_T}{S}\psi_{21}; \quad 3 \le F_n \le 4 \quad (19)$$

where $F_n = F_n$ (number of baffles, baffle spacing ratio). Comparison of equations (17) and (19) yields

$$\bar{b} = [F_n/2 - 2] \quad (20)$$

Symmetry of the 2 x 2 stiffness matrix implied by equations (17) and (18) requires that

$$\bar{a} = 3\bar{b}/S = 1.5\,F_n/S - 6/S \quad (21)$$

Therefore, for the shell side tubing, we have the final relations

$$H_{3T} = \frac{2E_T I_T}{S^3}[(\tfrac{9}{2}F_n - 12)\bar{V}_3 + 3S\psi_{21}(F_n/2 - 1)]$$
$$M_{3T} = \frac{2E_T I_T}{S^3}[3S\bar{V}_3(F_n/2-1) + F_n/2\,S^2\psi_{21}] \quad (22)$$

We now relate kinematic variables describing tube response to plate deformation

variables by noting that in accordance with sign conventions implied by Figs. 2 and 3, we have

$$\bar{V}_1 = U_{01} + (h_1/2)\theta_1; \quad \bar{V}_2 = U_{02} - (h_2/2)\theta_z$$

$$\bar{V}_3 = U_{02} + (h_2/2)\theta_2; \quad \psi_{11} = -dw_1/dr \tag{23}$$

$$\psi_{12} = -dw_2/dr = \psi_{21}$$

Note that we assume that the tube and plates have equal displacement values at the respective plate surfaces. Also, we assume that the tube centerline remains perpendicular to the local tubesheet surface. In the model herein, we make no attempt to describe the tube region within each tubesheet.

Finally, we note that the tube axial force, F_{1T}, in the region between the two tubesheets, and the tube axial force, F_{2T}, in the shell side tubing is related to the lateral deformation of the tubesheet by

$$F_{1T} = E_T A_T (w_2 - w_1)/L; \quad F_{2T} = -E_T A_T w_2/L_2 \tag{24}$$

Note that in this study, we have neglected thermal growth in the tubing, although these effects may be included with no added difficulty.

We consider now the case of a double tubesheet heat exchanger subjected to tube-side pressure p_1, shell side pressure p_3, and pressure p_2 in the gap between the two closely spaced tubesheets. We introduce the concept of tubesheet solidity λ by considering the representative repeated element of the tubesheet shown in Fig. 4 and forming

$$\lambda_i = 1 - A^{(i)}_{HOLE}/A; \quad i = 1,2 \tag{25}$$

It can then be shown that the following relationships are valid

Tubesheet #1

$$q_{\ell 1} = \lambda_1 p_1; \quad m_{\ell 1} = \tau_{\ell 1} = 0 \tag{26}$$

$$q_{u1} = -\lambda_2 p_2 + F_{1T}/A; \quad m_{u1} = M_{1T}/A; \quad \tau_{u1} = H_{1T}/A$$

Tubesheet #2

$$q_{\ell 2} = \lambda_2 p_2 - F_{1T}/A; \quad m_{\ell 2} = M_{2T}/A; \quad \tau_{\ell 2} = -H_{2T}/A \tag{27}$$

$$q_{u2} = -\lambda_2 p_3 + F_{2T}/A; \quad m_{u2} = M_{3T}/A; \quad \tau_{u2} = H_{3T}/A$$

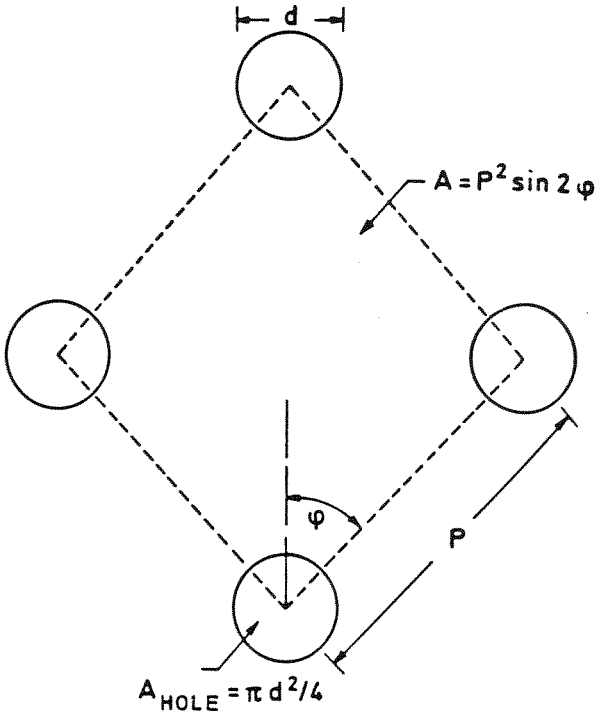

Fig. 4 Tubesheet layout

SOLUTION PROCEDURE

We use equations (11) through (12) to eliminate $N_{\theta i}$, M_{θ_i} from the equilibrium equations (2) through (4). The resulting equations, together with the constitutive equations (6), (8), and (13) are then cast as a system of 12 coupled first-order ordinary differential equations involving six force and moment resultants, and six deformation variables describing the state of strain in the tubesheet. The surface loadings, τ, m, and q, are expressed in terms of the tubesheet kinematic variables by equations (26 through 27), and the previously cited equations for tube forces and moments.

In matrix form, the field equations may be written in the final form

$$\frac{d}{dr}\{Z\} = [A]\{Z\} + \{B(p)\} + \{C(T)\} \tag{28}$$

where the dependent variable matrix $\{Z\}$ is given as

$$\{Z\}^T = [V_1, V_2, N_{r1}, N_{r2}, M_{r1}, M_{r2}, U_{01}, U_{02}, \theta_1, \theta_2, w_1, w_2] \tag{29}$$

The matrix $[A]$ is a 12 x 12 square matrix involving the independent variable, r, and various geometric and material properties of the system. The column matrices $\{B(p)\}$, $\{C(T)\}$ represent

the contribution of the applied mechanical and thermal loadings. Associated with equation (29) are six boundary conditions at r = 0 required by symmetry and finiteness of the solution.

$$V_1 = V_2 = U_{01} = U_{02} = \theta_1 = \theta_2 = 0 \quad \text{at} \quad r = 0 \tag{30}$$

and six additional boundary specifications at the outer tubesheet limit r = a. It is quite likely that at r = a, the boundary conditions themselves will include some interaction effects between the tubesheets, for small gap spacing, which depend upon actual construction details. In this work, however we use only classical plate-type boundary conditions which involve no coupling effects (i.e., pinned, clamped, etc.); thus our results obtained herein will focus attention only on the effect of tubesheet coupling inherent in the field equations.

Equations (29), together with properly specified boundary conditions, are solved by replacing the boundary value problem by a series of initial value problems, and then employing a direct numerical integration scheme. This technique is well documented in the literature on elastic shell theory (see Reference (7) for a complete discussion of the procedure and for additional source material). The particular solution algorithm used in this work is described in Reference (8).

APPLICATION TO TYPICAL DOUBLE TUBESHEET

The many geometric and material parameters involved in the simulation precludes any comprehensive parameter study in this initial work. Rather, we consider a specific configuration and content ourselves initially with an investigation into the effect of gap spacing L, and boundary conditions at r = a, on critical stresses in the various configuration components. We assume the following double tubesheet assemblage for the subsequent numerical example:

Tubesheet 1

$E_1 = 30 \times 10^6$ psi (206.8×10^9 N/m^2);

$n_1 = E_1^*/E_1 = 0.3$; $\nu_1 = 0.28$; $h_1 = 1$" (2.54 cm);

$\alpha_1 = 9.3 \times 10^{-6}$ (in/in°F); Shell radius a = 20" (.508 m) (31)

Tubesheet 2

$E_2 = 30 \times 10^6$ psi (206.8×10^9 N/m^2); $n_2 = E_2^*/E_2 = 0.3$; (32)

$\nu_2 = 0.28$; $h_2 = 1$" (2.54 cm); $\alpha_2 = 6.3 \times 10^{-6}$ (in/in°F)

Tubes

Pitch (diagonal) = 1.25" (3.175 cm); tube metal thickness = 0.049" (.124 cm); tube O.D. = 1" (2.54 cm); S = 40" (1.016 m)

$E_T = 30 \times 10^6$ psi (206.8×10^9 N/m^2); $L_2 = 200$" (5.08 m) (33)

Loading

$p_1 = 100$ psi (6.8948×10^5 N/m^2); $p_2 = p_3 = 0$

$T_1 = T_2 = 100$°F

We consider initially the case of mechanical loading only. As boundary conditions for the outer rim of the tubesheets, we assume, at r = a,

$$N_{r1} = N_{r2} = \theta_1 = \theta_2 = w_1 = w_2 = 0 \tag{34}$$

That is, we assume that the outer rim of both tubesheets is restrained against lateral deformation and cross-section rotation, but is free to expand radially. Numerical solution of the foregoing configuration has been obtained for various tubesheet gaps L in the range

$$10" \ (25.4 \text{ cm}) \geq L \geq 0.5" \ (1.27 \text{ cm}) \tag{35}$$

Some results of the study are shown in Fig. 5, where various force and moment result-

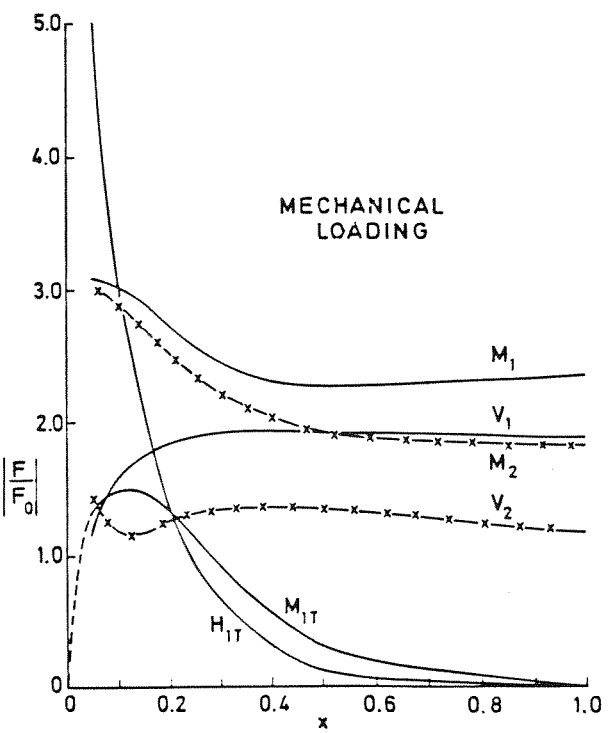

Fig. 5 Force and moment resultants versus separation for mechanical loading

ants at r = a are plotted against the dimensionless gap variable

$$x = L/L_o; \quad L_o = 10" \ (25.4 \text{ cm}) \tag{36}$$

In order to plot all of the results on the same scale, the vertical axis of Fig. 5 represents the absolute values of any of the dimensionless quantities

$$M_i/M_o; \quad V_i/V_o; \quad H_{iT}/H_{To}; \quad M_{iT}/M_o \tag{37}$$

where M_i, V_i, H_{iT}, M_{iT} are defined in Fig. 2 for the i^{th} tubesheet, and in Fig. 3 for the tubes. The reference values, M_o, V_o, H_{To}, for plotting purposes are taken as

$$\begin{aligned} M_o &= 100^{\text{in}\#}/\text{in} \ (444.82 \text{ N-m/m}) \\ V_o &= 100^{\#}/\text{in} \ (1.7513 \times 10^4 \text{ N/m}) = H_{To} \end{aligned} \tag{38}$$

Fig. 5 shows, for the loading p_i = 100 psi (6.8948×10^5 N/m^2), the critical stress resultants at r = a, as a function of the gap between the tubesheets. The curve for tube moment M_{1T} has been extended to zero gap spacing since it is clear that the tube bending moment must approach zero as the gap is eliminated. The tube shear force, H_{1T}, must also approach a finite value for zero gap, but the numerical simulation was not carried to a small enough gap so that this limit could be ascertained. From a practical point of view, it appears that the lower limit of gap spacing investigated is sufficient for most contemplated designs. Once tube forces and moments are determined, stress levels in the various components are easily identified. For example, from the results shown in Fig. 5, the maximum shear stress in the tubes (due to H_{1T}) and the axial stress in the tubes (due to M_{1T}) is obtained as

$$\begin{aligned} \tau &= 2\frac{H_{1T}}{A_T} = 6776.4 \text{ psi} \ (46.722 \times 10^6 \text{ N/m}^2) \\ \sigma_a &= \frac{M_{1T}d}{2I_T} = 3924 \text{ psi} \ (27.056 \times 10^6 \text{ N/m}^2) \end{aligned} \tag{39}$$

for a gap of 0.5 in. (1.27 cm). The bending stress at the rim of tubesheet 1 may be found from the relation (note that in an actual design case tubesheet stresses are scaled up by the inverse of the ligament efficiency in the perforated region)

$$\sigma_B = \frac{6M_1}{h_1^2} = 1848 \text{ psi} \ (12.742 \times 10^6 \text{ N/m}^2) \tag{40}$$

It may be of interest to point out that if tubesheet 2 were eliminated, the bending stress, σ_B, is found to increase by the factor 10.9.

Although not shown in the graph, the shear transfer between the tubesheets, for the case of small separation, allows the double tubesheet assemblage to resist gross lateral movement by developing direct compressive forces in tubesheet 1, and direct tensile forces in tubesheet 2. These direct radial forces are negligible near r = a because of the specified boundary conditions on radial deformation, and reach their maximum value at the center of the tubesheets. For the configuration at hand, for a separation between tubesheets of 1.27 cm, a direct radial stress of 168 psi (1.158×10^6 N/m) results at r - 0. Our remark following equation (40) shows that for mechanical loading only, significant stress reduction in the tubesheets is obtainable. However, from a practical point of view, further reduction of tubesheet thickness may be undesirable from a manufacturing and assembly standpoint.

A more interesting set of results is obtained for the case of purely thermal loading of the tubesheet configuration. We develop a thermal driving force by specifying different thermal expansion coefficients, but the same temperature rise for both tubesheets. It is clear from the equations that the numerical results shown in Fig. 6 are valid for any thermal driving force as long as the combinations, $\alpha_1 T_1, \alpha_2 T_2$, remain unchanged.

Fig. 6 shows the variation of relevant force and moment resultants, that appear critical for design purposes, as a function of tubesheet gap. Reference value for M_o, V_o, H_{To} are given by equation (38), and the initial set of results is obtained for the boundary conditions used for the case of mechanical loading only. The results obtained for thermal loading indicate that changes in values of the forces and moment resultants, as tubesheet separation decreases, are considerably more severe than in the case of mechanical loading. It is clear, however, that the design of a double tubesheet configuration with a small separation between tubesheets is possible; from the results shown in Fig. 6, it appears that the direct shear stress in the tubes due to

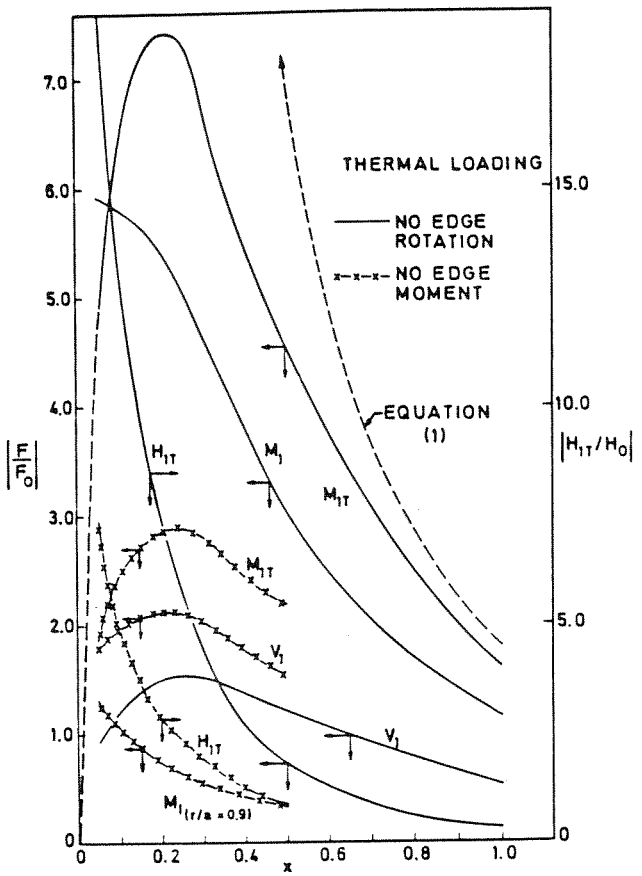

Fig. 6 Force and moment resultants versus separation for thermal loading

the force H_{1T} will probably govern the design.

For the configuration studied, we have also plotted results for the tube bending moment that are implied by using equation (1) and solving for the stress for a given separation, L. The results show the expected conservative nature of equation (1) when the tubesheet separation is large, and also indicate the departure from reality that results if equation (1) is applied to a configuration where significant tubesheet interaction occurs.

As an initial attempt to assess the possible effect of different plate boundary conditions on the results of interest for design, we reconsider the double tubesheet configuration under thermal driving load, and replace the boundary conditions given in equation (34) by the boundary conditions at r = a given in the following:

$$N_{r1} = N_{r2} = M_{r1} = M_{r2} = w_1 = w_2 = 0 \qquad (41)$$

That is, we presumably make the system somewhat more flexible by allowing cross-section rotation to occur at the outer edge of both tubesheets. Fig. 6 shows some results of interest which occur for this set of edge conditions. Of significance to contemplated designs is the fact that tube shear forces and bending moments decrease dramatically; it is clear that this might have been expected since, in a thermal loading situation, one can generally surmise that an increase in system flexibility will decrease the thermal stresses.

CONCLUDING REMARKS

The governing equations for a symmetrically loaded double tubesheet configuration of circular planform have been formulated and a solution procedure devised and illustrated. The prime motivation for this work has been to clearly point that the design of a double tubesheet configuration having gap spacing on the order of one or two tube diameters is certainly feasible, but requires a rigorous analysis in order to insure structural integrity in service under mechanical and thermal loading. The results obtained for the single configuration studied imply that stress due to thermal loadings are more sensitive to the tubesheet separation. In any specific design example, the numerical simulation can be used to obtain maximum force and moment resultants in all critical areas. If desired, extensive parametric studies can be carried out to ascertain the effect on the design of varying one or more of the geometric or material parameters.

In closing, we point out that a major impetus for carrying out this study has been a possible application of double tubesheets to large power plant condensers. The particular application discussed, however, was limited to a relatively small circular unit. Because of the numerical solution method used in this work, which requires that a boundary value problem be changed to a series of initial value problems, the solution method becomes extremely sensitive to the ratio, L/a, in the presence of the elastic foundation effect. For L/a too small, the solution procedure gives incorrect results; during the course of the solution, subtraction of nearly equal large numbers occurs and all control of error disappears. The occurrence of this difficulty has long been recognized by the users of this solution procedure (7), and extensions of the technique to overcome this problem are well

established. We note only that the present computer simulation of the double tubesheet problem also experiences this effect. To apply the method to large power plant condenser configurations requires the incorporation of a more elaborate direct solution technique incorporating "multi-segments" (7), so that very small L/a values can be modeled. However, we emphasize that the basic field equations and the general trend of the results are as presented in this work; therefore, the results presented here stressing the problem formulation and application are of lasting interest. While it is true that any particular configuration can be studied using a finite element code, the direct integration method presented in this work provides a cost-effective vehicle for detailed parametric studies to establish the relative importance of the various geometric and material parameters.

REFERENCES

1 Peake, C. C., Gerstenkorn, G. F., and Arnold, T. R., "Some Reliability Considerations - Large Surface Condensers," paper presented at the 1975 American Power Conference, Chicago, Ill., April 1975.

2 Yokall, S., "Double Tubesheet Heat Exchanger Design Stops Shell Tube Leakage," Chemical Engineering, May 1973, pp. 133-136.

3 Zudans, Z., Yen, T. C., and Steigelmann, W. H., Thermal Stress Techniques in the Nuclear Industry, Chapter 5, American Elsevier Co., New York, 1965.

4 Cook, R. D., "A Mechanical Analysis of Coupled Tube Sheets," Univeristy Microfilm, Inc., Ann Arbor, Mich., 1963.

5 Severn, R. T., "Inclusion of Shear Deflection in the Stiffness Matrix for a Beam Element," Journal of Strain Analysis, Vol. 5, No. 4, 1970, pp. 239-241.

6 Gardner, K. A., "Heat Exchanger Tubesheet Design," Journal of Applied Mechanics, Vol. 15, Transactions ASME, Vol. 70, 1948, p. A-377.

7 Kraus, H., Thin Elastic Shells, Wiley, 1967, pp. 419-430.

8 Hutchins, G. J., and Soler, A. I., "New Results on Application of Multi-Segment Stepwise Integration of First Order Equations," Journal of Computer Methods in Applied Mechanics and Engineering, 1972, pp. 307-316.